Biogenic synthesis and comparative assessment of the antimicrobial activities of silver and zinc nanoparticles of *Dialium guineense* leaf extract against human pathogens

ABSTRACT

Aim: The study aimed to perform a comparative evaluation of the antimicrobial activities of green synthesis of silver and zinc nanoparticles.
Study design: Experimental.
Methodology: A biogenic and facile method of synthesis of silver and zinc oxide nanoparticles (DGL—SNPs and DGL—ZNPs) using silver nitrate and zinc nitrate as precursors and an aqueous extract of *Dialium guineense* leaf (DGL) as a reducing agent respectively was demonstrated in this work. The synthesized DGL—SNPs and DGL—ZNPs were checked for their antimicrobial activity against strains of *Staphylococcus aureus, Escherichia coli, Pseudomonas aeruginosa, Proteus mirabilis, Klebsiella pneumoniae, Streptococcus pneumoniae and Candida albicans.* Comparative assessment of the antimicrobial activities of DGL—SNPs and DGL—ZNPs against human pathogens were also conducted.. Characterization of the metallic nanoparticles were carried out by UV-visible spectroscopy, Fourier transforms infrared spectroscopy (FT-IR), Scanning electron microscope (SEM), powder X-ray diffraction (XRD), Energy dispersive X-ray (EDX), as well as the BET (Brunauer-Emmett-Teller) surface area measurement.
Result: Both metallic nanoparticles were found to inhibit the growth of microbes. However, One-way ANOVA of the IC50 of microbial growth inhibition profile shows significant mean difference between DGL—SNPs and DGL—ZNPs; DGL—SNPs showed improved outcome to the DGL—ZNPs with a P value of 8×10^{-4} at $P < 0.05$. The surface Plasmon resonance absorption peak of 275 and 261 nm for DGL—SNPs and DGL—ZNPs respectively; FTIR analysis revealed the presence of phytochemicals such as phenol, saponin, and alkaloid that play the major roles in stabilizing the DGL—SNPs and DGL—ZNPs. XRD result shows a crystallite size of 27.9 nm and 22.6 nm from the width of the principal peak reflection of (0 1 3) and (1 2 2) respectively for DGL—SNPs and DGL—ZNPs; EDX shows the formation of Silver atoms and ZnO in the DGL—SNPs and DGL—ZNPs; from the BET, the average particle size 59.76 nm for silver and 70.17 nm for zinc. The SEM showed the irregular structure of DGL—SNPs and DGL—ZNPs.
Conclusion: There is a significant difference in the antimicrobial properties of silver nanoparticles and zinc nanoparticles as a promising agent against human pathogens.

Keywords: ANOVA, *Antimicrobial activity, BET, EDX, FTIR, Green synthesis, IC_{50}, IZD, SEM, Silver Nanoparticles,* Treatment–control (T/C) ratio, *XRD, Zinc oxide Nanoparticles*

1. INTRODUCTION

The inappropriate and excessive use of broad-spectrum antibiotics has resulted in a significant increase in antimicrobial resistance, posing a serious threat to human health. This situation necessitates the development of novel antibacterial agents that employ more effective mechanisms of action (Shaalan *et al.,* 2017; Filho *et al.*, 2023). The overutilization of antibiotics plays a critical role in this crisis, as antimicrobial resistance (AMR) genes can be transferred among microorganisms in humans, animals, and aquatic organisms (Shaalan *et al*., 2017; Gugale *et al*., 2021).

Experts have identified this challenge as a global health emergency, as numerous infections—such as otitis media, urinary tract infections, sexually transmitted infections like gonorrhoea, pneumonia, tuberculosis, and various wound infections—are now caused by organisms resistant to one or more antibiotics. The extensive research conducted by Murray and colleagues has provided a thorough overview of the burden of AMR (Raja *et al*., 2023). Their findings indicate that approximately 4.95 million deaths in 2019 were associated with bacterial AMR. Notably, several antimicrobial-resistant microorganisms, including *Escherichia coli,*

Staphylococcus aureus, Klebsiella pneumoniae, Streptococcus pneumoniae, Acinetobacter baumannii, and *Pseudomonas aeruginosa*, contributed to these fatalities. Specifically, methicillin-resistant *Staphylococcus aureus* accounted for over 100,000 of these deaths in 2019 (Raja *et al.,* 2023).

Despite the considerable advancements in antibiotic development over recent decades, there has yet to be a significant enhancement in antimicrobial activity specifically targeting multidrug-resistant bacteria (Raja *et al.,* 2023). The emergence of these resistant strains, along with the substantial healthcare costs associated with their management, emphasizes the critical necessity for the formulation of novel and effective antimicrobial strategies aimed at combating infectious diseases and mitigating resistance. Microorganisms exhibit a remarkable capacity to adapt to evolving environments, leading to the rapid development of resistance against antimicrobials, particularly those that function through a defined mode of action, such as conventional antibiotics. Therefore, it is of paramount importance to pursue the innovation of novel antimicrobials characterized by both efficacy and a nonspecific mode of action, as this represents a viable and promising avenue for addressing the challenges posed by antimicrobial resistance ((Gugale *et al*., 2021; Raja *et al.,* 2023).

Metallic nanoparticles possess the capability to non-specifically eliminate bacterial cells by targeting various cellular components. The antimicrobial efficacy of these nanoparticles is significantly influenced by their size; typically, bacterial cells measure in the micrometre range, while the pores within their membranes are on the nanometre scale. This discrepancy indicates that the antimicrobial activity of nanoparticles is not solely attributed to the release of free metal ions, but also to their high surface area-to-volume ratio, which facilitates close interactions with microbial membranes. Additionally, the relatively non-specific mode of action exhibited by metal nanoparticles diminishes the rate of resistance development, positioning them as promising alternatives to traditional antimicrobials.

Numerous studies have investigated the antimicrobial effectiveness of metal and metal oxide-based nanoparticles against various bacterial strains (Ma *et al.,* 2022; Raja *et al*., 2023; Mondal *et al.*, 2024; Shnawa *et al.,* 2024). Notable examples include copper, silver, zinc, cobalt, titanium, chromium, lead, mercury, and gold (Salazar-Aleman and Turner, 2022; Mirel *et al.,* 2022). However, due to their inherent toxicity, nanoparticles composed of mercury and lead have largely been avoided in practical applications (Crane 2020). Copper, recognized for its long-standing antimicrobial properties, is widely utilized in drinking water treatment and distribution. In 2008, the United States Environmental Protection Agency designated copper as the first metallic antimicrobial agent (Vincent *et al*., 2016). Similarly, zinc oxide and magnesium oxide nanoparticles have demonstrated promising antimicrobial effects; ZnO nanoparticles have shown efficacy in combating both *Staphylococcus aureus* and *Escherichia coli in vitro* (Raja *et al.,* 2023; Shnawa *et al.,* 2024).

Metallic nanoparticles, such as Silver nanoparticles (Ag NPs) and zinc oxide nanoparticles (ZnO NPs) have attracted considerable interest due to their application as antimicrobial agents in various fields, including dental implants, catheters, and the treatment of burn wounds (Okeniyi *et al.,* 2017; Gugale *et al*., 2021; Karade *et al.,* 2021; Raja *et al.,* 2023). As inorganic antibacterial entities, Ag NPs present significant potential within the pharmaceutical and medical sectors for a wide range of biological applications. These nanoparticles serve as antifungal and antibacterial agents, particularly effective against antibiotic-resistant organisms, thereby offering valuable options for infection prevention (Kim *et al.,* 2007; Yoo *et al*., 2021).

They can be synthesized using several well-established techniques, including chemical reduction, physical vapour deposition, and biological methods. A particularly noteworthy approach is the green synthesis of silver nanoparticles, which utilizes plant constituents such as sugars, fats, flavonoids, alkaloids, and polyphenols. This method emerges as a sustainable alternative to conventional chemical formulations (Okeniyi *et al.,* 2017; Rather *et al.,* 2021). In their work, "Effect of *Dialium guineense* based zinc nanoparticle materials on the inhibition of microbes inducing microbiologically influenced corrosion [*MIC*]", Okeniyi and co-workers demonstrated the effects of extracts of the leaf of the plant as precursor zinc nanoparticle material. Results showed that the biomaterial capped nanoparticle exhibited inhibited growth of the studied different *MIC* inducing microbes (Okeniyi *et al.,* 2017).

The principal mechanism of antimicrobial action of Ag NPs is predicated on the release of silver ions that disrupt microbial cellular processes. This disruption occurs through various pathways, including the compromise of cell membrane integrity, deactivation of critical enzymes, and inhibition of DNA and RNA synthesis (Gao *et al*., 2018; Mondal *et al.,* 2024). Ag NPs are characterized by their excellent electrical and thermal conductivity as well as their pronounced antimicrobial properties, making them particularly

advantageous in applications such as wound dressings, antimicrobial coatings, and water purification systems. Moreover, the size and shape of these nanoparticles can be meticulously controlled during synthesis to customize their properties, thereby enhancing their broad-spectrum antimicrobial activities for specific applications.

Among the various categories of metal-based nanoparticles, zinc oxide nanoparticles (ZnO NPs) represent one of the most extensively investigated entities. ZnO NPs are distinguished by their stability at the elevated temperatures and pressures commonly encountered in food processing environments, and they are widely regarded as safe for application ((Okeniyi *et al.,* 2017; Yoo et al., 2021). Composed of zinc and oxygen atoms, these nanoparticles generally possess dimensions ranging from 1 to 100 nanometres. Zinc oxide itself is constituted by zinc cations (Zn^{2+}) and oxide anions (O^{2-}).

At the nanoscale, the properties of materials may diverge significantly from those of their bulk counterparts, and ZnO nanoparticles exhibit unique characteristics that render them valuable for a wide range of applications. The activity of these nanoparticles is frequently attributed to the generation of reactive oxygen species (ROS) on their surfaces, which can induce oxidative stress in microbial cells. Zinc oxide nanoparticles are routinely utilized in sunscreens and cosmetics due to their capacity to block ultraviolet radiation, in addition to their antimicrobial properties. Furthermore, they display a high degree of biocompatibility and are subject to extensive research within the fields of medicine and pharmaceuticals, particularly concerning tissue engineering and drug delivery applications (Dizaj *et al*., 2014; Ma *et al.,* 2022; Mondal *et al.,* 2024).

Numerous approaches for the synthesis of nanoparticles have been proposed, which can be primarily categorized into three groups: physical, chemical, and biological methods. Currently, physical and chemical techniques dominate the production of nanoparticles. While these methods ensure a continuous supply, they also come with significant drawbacks, including high energy consumption and the generation of toxic by-products. This situation underscores the necessity for sustainable and environmentally friendly synthesis methods.

In response to these challenges, the biosynthesis of metallic nanoparticles has gained increasing attention due to its economic viability, reduced toxicity, and the simplicity of the process. This method facilitates the development of nanoparticles with consistent size, shape, and mono-dispersity (Punjabi et al., 2018). Notably, bio-synthesized silver nanoparticles (Ag NPs) and zinc oxide nanoparticles (ZnO NPs) have demonstrated effective antimicrobial properties, positioning them as promising candidates for future antimicrobial agents and the development of innovative therapeutic drugs (Dilek *et al.,* 2019).

The antimicrobial properties of various metallic nanoparticles have been well-documented; however, it is crucial to recognize that not all metallic nanoparticles have the ability to target and eliminate every type of bacteria (Bankier *et al*., 2019). A comparative analysis of the antimicrobial efficacy of diverse metallic nanoparticles is essential, as each type may exhibit different levels of effectiveness against specific bacterial strains. This variability is influenced by several factors, including size, shape, surface chemistry, and composition. Consequently, certain nanoparticles may show significantly higher potency against particular pathogens compared to others (Kalakonda *et al*., 2024). These insights allow researchers to identify the most appropriate nanoparticles for targeted applications in healthcare and other sectors that demand antimicrobial activity, while also considering potential toxicity and environmental impact (Bankier *et al*., 2019; Kalakonda *et al.*, 2024). Therefore, this study intends to undertake a comparative evaluation of the antimicrobial activities of silver and zinc nanoparticles synthesized through environmentally friendly methods utilizing extracts from *Dialium guineense* leaves.

2. Methodology

2.1 Materials

All the reagents were of analytical grade and used as received without further purification. Anhydrous silver nitrate, $AgNO_3$ (99.8%), DMSO, Zinc nitrate, $Zn(NO)_3$, Mueller-Hinton agar and Sabourands dextrose agar (SDA) were obtained from Sigma Aldrich (Germany). Standardized test isolates of the fungus *Candida albicans* and some selected Gram positive bacterial strains of were obtained from the Pharmaceutical

Microbiology Laboratory, Enugu State University of Science and technology. All the aqueous solutions were prepared using distilled water (DW).

2.2. Collections of *Dialium guineense* leaves (DGL)

The leaves of *Dialium guineense* plant were freshly obtained from within the University environment of Enugu State University of Science and Technology, Agbani, Nkanu West Local Government Area of Enugu State, without causing any damage to the plant. An attempt was made to identify and authenticate the plant by comparing the leaves and pods with those identified by Marco Schmidt (https://orcid.org/0000-0001-6087-6117) (iNaturalist, 2024) and deposited at the Herbarium Centre, Department of Pharmacognosy, Enugu State University of Science and Technology, with a voucher number: FP/Cog/18020.

2.3. Preparation of DGL

The leaves of *Dialium guineense* Willd, were thoroughly washed using distilled water, spread on a white Formica board to dry at room temperature for 96 h. This was then followed by a reduction in the particle size using a mechanical grinder into a fine powder. The powder was extracted in hot water as described in Aisida *et al.* (2019): 100 g of the plant powder was dissolved in 500 mL of distilled water (DW) followed by heating at 80℃ for 1 h, after which the system was allowed to cool to room temperature. The mixture was filtered using a sieve followed by Whatman No. 1 filter paper. The filtrate was decanted and preserved in a refrigerator at a temperature of 4℃ for further usage.

2.4. Biogenic synthesis of silver and zinc oxide nanoparticles (DGL—SNPs and DGL—ZNPs)

All beakers and cylinders were thoroughly cleaned and autoclaved before use and deionized water was used for the synthesis. Silver nanoparticles synthesis was carried out by the chemical reduction method as previously described in Aisida *et al.* (2019) with slight modification. The mass equivalent in g of 0.05 M of silver nitrate were weighed and dissolved in 100 mL of sterile water followed by continuing stirring for 1 h using a magnetic stirrer to ensure uniform dissolution. 50 mL of DGL extract was then added drop-wise to 50 mL of the respective precursor salt solutions to achieve a 1:1 volume ratio for each system, while stirring at room temperature for another 2 h to form a homogenous solution. The homogenous solution was centrifuged at 1500 rpm for 10 minutes. The obtained silver nanoparticles of *Dialium guineense* leaves (DGL—SNPs) were washed severally with DW and dried in hot air oven for further characterization. The sample was labelled as DGL—SNPs and stored in a glass vial placed in a dark box as silver nanoparticles are sensitive to light at room temperature.

Similarly, the mass equivalent in g of 0.05 M of zinc nitrate was weighed and dissolved in 100 mL of sterile water as described in the synthesis of DGL—SNPs. Zinc nanoparticles from DGL were also prepared following the steps described above to obtain zinc nanoparticles of *Dialium guineense* leaves (DGL—ZNPs). The sample was labelled as DGL—ZNPs.

The biosynthesis enhanced the reduction of $Ag^{+}$to Ag^{0}atoms, and Zn^{2+} to Zn^{0} from the supernatant of the enzymatic extract of DGL as shown in equation 1 and 2 respectively.

$$Ag^{+} + e^{-}(phytochemical\ enzymes) \rightarrow Ag^{0} \quad \ldots\ldots\ldots\ldots\ldots\ldots\ldots\ldots\ldots (1)$$

$$Zn^{2+} + 2e^{-}(phytochemical\ enzymes) \rightarrow Zn^{0} \quad \ldots\ldots\ldots\ldots\ldots\ldots\ldots\ldots (2)$$

2.5. Characterization of DGL—SNPs and DGL—ZNPs

The BET (Brunauer -Emmett -Teller) surface area measurement was made using a conventional BET multi-point N_2 physisorption apparatus (Gemini 2360, Micromeritics Instruments Corp). The N_2 adsorption was measured from a six-point isotherm in a relative pressure rang of 0.05 to 0.3 at 77.3 K. The assumption for the cross-sectional area of N_2 was taken to be 16.2 $Å^2$ (Zou *et al.*, 2020) and the density used was 3.65 g/cm^3. The sample was prepared by heating at 150℃ for 1 hr. while simultaneously a flow of N_2 gas across the sample tube seeps away the liberated contaminants. The average particle diameter was calculated using the formula in Eq. (3)

$$Average\ particle\ diameter\ (nm) = \frac{6000}{BET\ surface\ area\ (m^2\ g^{-1}) \times density\ (g\ cm^{-3})} \ldots\ldots\ldots (3)$$

The surface morphologies of the samples were obtained using a scanning electron microscope (SEM). The Thermoscientific Energy Dispersive X–ray Spectrometer (EDX) was used for elemental analysis. A Fourier transforms infrared spectrophotometer (FTIR) was used for the determination of the surface functional groups. Also, the absorption was determined by UV-vis spectrophotometer in the wavelength range of 200–1000 nm.

The structural studies of silver nanoparticles and zinc nanoparticles formed from the respective green synthesis of SNPs and ZNPs using the leaves extract of *Dialium guineense* were studied using the powder X–ray diffractometer with Cu-Kα radiation (λ = 1.5406 Å) and lattice parameter (a = 4.08620 Å) at room temperature in the continuous scanning mode and a scanning 2θ range of 15– 80°.

2.6. Antimicrobial activity of DGL—SNPs and DGL—ZNPs

The test agents, DGL—SNPs and DGL—ZNPs were evaluated for their antimicrobial activities against strains of *Staphylococcus aureus, Escherichia coli, Pseudomonas aeruginosa, Proteus mirabilis, Klebsiella pneumoniae, Streptococcus pneumoniae and Candida albicans.* using the DGL aqueous extract (AE), as placebo. The agar well diffusion method as described by Adonu (2023) was used with slight modification. Two fold dilutions of the agents were prepared in DMSO ranging from 100–12.5 mg/mL. Twenty millilitre each of molten Mueller-Hinton agar and Sabourands dextrose agar (SDA) was seeded with 0.1 ml of standardized broth cultures of the test bacteria and *Candida albicans* respectively. A total of 6 wells, 8 mm in diameter were made in each of the agars using a sterile corkborer. A 0.05 ml each of the two-fold dilutions of the agent was added into each labelled hole using a sterile pipette. As a control, a 0.05 ml DMSO was put in the last well. The plates were left for 1 h at room temperature for diffusion after which they were incubated at 37℃ for 24 h. The diameter of the zone of inhibition (IZD) was measured at the end of the incubation period. Each data point are the mean values of three replicates of IZD determinations.

Furthermore, the evaluation of minimum inhibitory concentration (MIC) of the agents DGL—SNPs and DGL—ZNPs against the organisms were tested. The MIC of each of the agents was determined using agar dilution method (CLSI, 2022). Five different dilutions of each of the agents were prepared by two-fold dilution. The ranges of the concentrations of the agent against the test isolates were 0.6 – 5.0 mg/ml. With an automatic micropipette, 1.0 ml each of these different dilutions (one dilution per plate) of the agent was introduced into individual agar plates. The molten agar and the agents were mixed carefully and thoroughly and allowed to set. With the aid of a sterile wire loop, the standardized test isolates were delivered on the agar surface of the plates containing different concentrations of the agent. This was done by streaking on the surface of the set agar. These inoculated agar plates were incubated at 37℃ for 24 h for bacteria and 25℃ for 48 h for the fungus. At the end of the incubations, the MICs were determined as the lowest concentration of the agent that allowed not more than one colony forming units (cfu) to grow in it. Again, each data point are the mean values of three replicates of MIC determinations.

Using the MIC obtained for DGL—SNPs and DGL—ZNPs treatment, a 12 hr. treatment for *P. mirabilis* was conducted in which the IZD was measured on hourly basis, after which the treatment–control (T/C) ratio

2.7. Statistical analysis

Microsoft Excel 2013 was used to calculate the average values of three replicates of IZD and MIC determinations, while GraphPad Prism 5 was used for the following treatment:

i. Normalizing the responses to percentages,
ii. Transforming the MIC to logarithmic value,
iii. Determining the IC_{50} and,
iv. Computing the One-way analysis of variance (ANOVA) of the antimicrobial activities of synthesized DGL—SNPs and DGL—ZNPs.

3. RESULT AND DISCUSSION

3.1. SEM and EDX analysis of DGL—SNPs and DGL—ZNPs

Figure 1 gives the surface morphology and elemental composition of the biosynthesized crystal samples. The analysis conducted using scanning electron microscope (SEM) demonstrated that the morphology of the

biosynthesised DGL—SNPs and DGL—ZNPs exhibited an irregular shape, with a well-dispersed, uniform size as well as crystalline structure. The EDX analysis identified that relative abundance of elements in the DGL—SNPs and DGL—ZNPs samples. For DGL—SNPs, the relative abundance of silver atom was about 43 %, and 41 % for DGL—ZNPs sample. The average particle size of DGL—SNPs was calculated as 59.76 nm, while that of the DGL—ZNPs had an average particle size of 70.2 nm (Figure 3a and b).

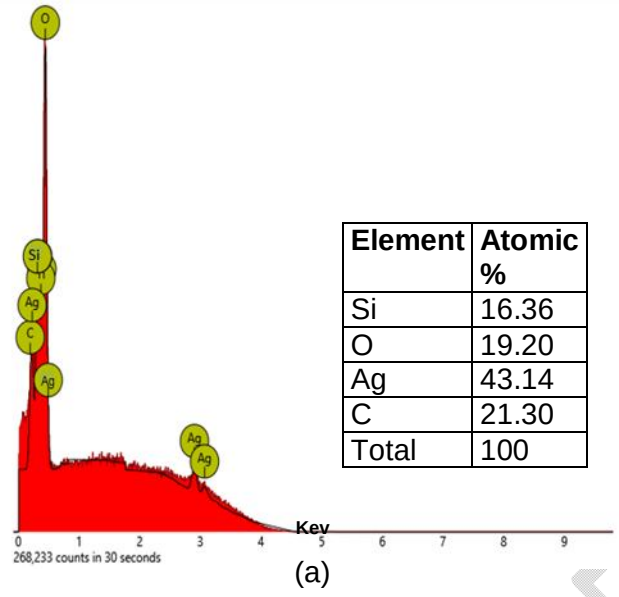

Element	Atomic %
Si	16.36
O	19.20
Ag	43.14
C	21.30
Total	100

(a)

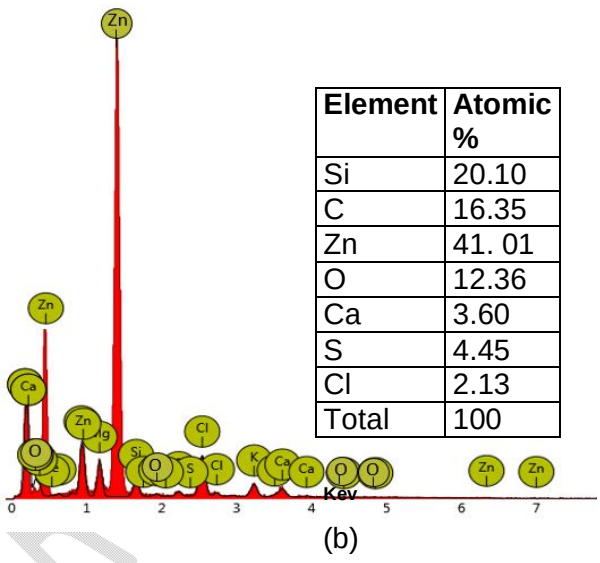

Element	Atomic %
Si	20.10
C	16.35
Zn	41. 01
O	12.36
Ca	3.60
S	4.45
Cl	2.13
Total	100

(b)

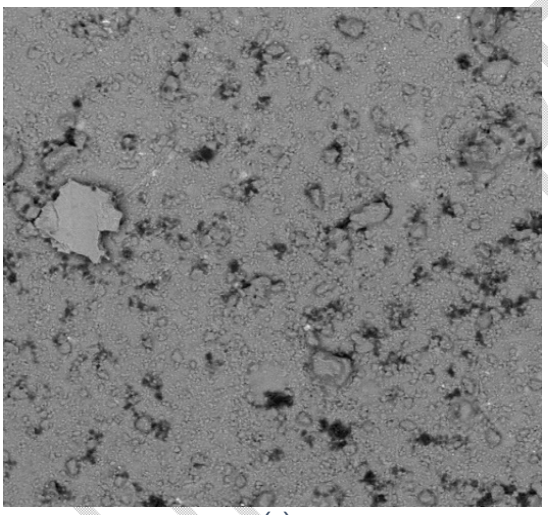

(c)

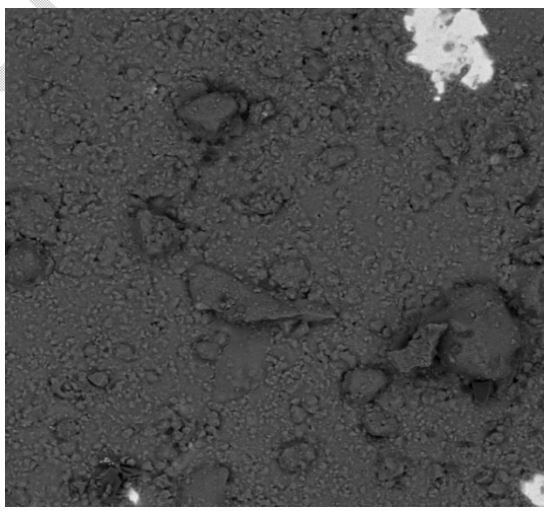

(d)

Figure 1. EDX of (a) DGL—SNPs (b) DGL—ZNPs ; and SEM images of (c) DGL—SNPs and (d) DGL—ZNPs

3.2. UV—Visible spectral analysis of DGL—SNPs and DGL—ZNPs

The absorbance of the samples showed a notable colour change corresponding to the reduction of pure silver and zinc metal ions into silver and zinc nanoparticles, respectively, facilitated by the reactive functional moieties present in DGL. Following the reaction, a discernible shift to a dark brown hue was observed, indicative of the interaction between the precursor and the reducing agent (Figure 2a and b). This process resulted in the emergence of surface Plasmon resonance (SPR) peaks at 261 nanometres for zinc and 275

nanometres for silver (Figure 2). The result obtained is not agreement with Aisida *et al* (2019) who reported an SPR for silver nanoparticles in the range of 390-490 nm. Also, Akpomie *et al* (2021) and Khan *et al* (2023) observed a UV—Vis absorption band at 375 nm and 311 nm for ZnO nanoparticles respectively. SPR in various nanoparticles is reportedly influenced by such characteristics as size, shape, electrical properties and compositions. This property of nanoparticles affects the plasmon absorption and its bandwidth (Marhaba, 2018; Pashazadeh-Panahi and Hasanzadeh, 2020). The particle sizes of DGL—SNPs and DGL—ZNPs were increased by treating with 2 M NaOH during the synthesis. This can explain the variation in SPR measurement.

Figure 2. UV—visible spectra showing the surface plasmon resonance exhibited by the metallic nanoparticles, SNPs and ZNPs. (a) reduction of silver ions to silver atoms by DGL (b) reduction of zinc ions to zinc atoms by DGL

3.3. XRD ANALYSIS OF DGL—SNPS AND DGL—ZNPS

The XRD analysis produced the pattern shown in Figure 3 (c) and (d). The analysis was used to determine phase purity and crystallinity of DGL—SNPs and DGL—ZNPs. The peaks observed at 2θ values of 12.54°, 21.10°, 25.22°, 26.86° and 50.34° with Card No.: 00-001-0649 could be corresponding to the crystallographic planes (011), (112), (022), (013) and (125) of the DGL_SNPs with face–centred cubic silver lattice. Conversely, the peaks observed at 2θ values of 12.26°, 24.92° and 26.66° with Card NO.: 00-003-0444 could be corresponding to the crystallographic planes (011), (022), and (122) of the DGL—ZNPs. The zinc oxide nanoparticle showed a crystalline and hexagonal wurtzite structure. The particle crystallite size for DGL—SNPs and DGL—ZNPs was determined as 27.9 nm and 22.6 nm from the width of the principal peak reflection of (013) and (122) respectively using the Debye–Scherer formula in Eq. (4). There were no characteristic peaks of impurities.

$$L = \frac{0.9\lambda}{\beta cos\theta} \ldots\ldots\ldots\ldots\ldots\ldots\ldots\ldots (4)$$

Where L is the crystallite size (nm), λ is the X-ray wavelength (λ = 1.5406Å), β is the half-width band of the diffraction band (FWHM) measured in radian, K is the shape factor, usually taken as about 0.89 and θ is the Bragg diffraction angle (Peak position in radians).

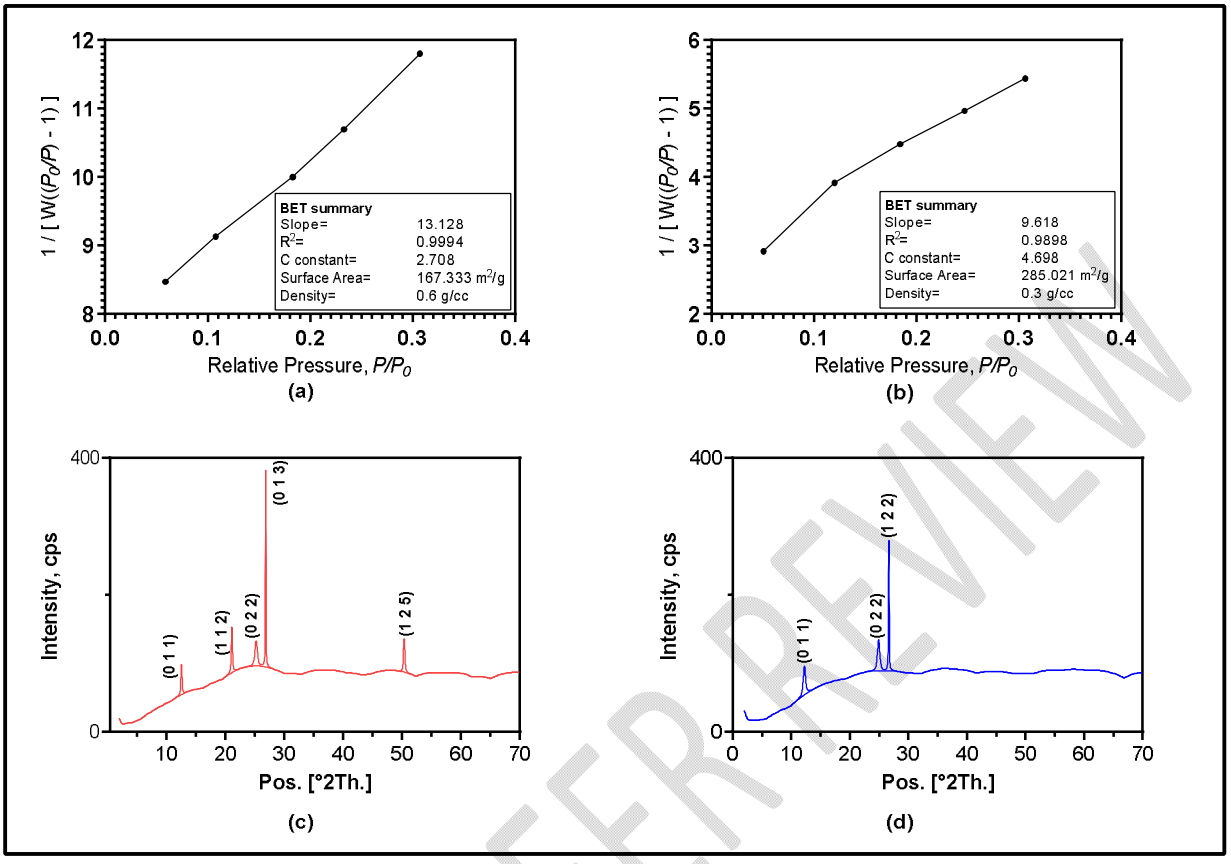

Figure 3. Multipoint BET plot, showing the surface area of (a) DGL—SNPs and (b) DGL—ZNPs; XRD pattern of (c) DGL—SNPs (d) DGL—ZNPs

3.4. FTIR spectra analysis of DGL—SNPs and DGL—ZNPs

FTIR spectroscopy was used to identify the possible biomolecules present in *Dialium guineense* leaf extract which are responsible for reducing the Ag^{+} to Ag^{0}, as well as Zn^{2+} to ZnO, capping and stabilizing the silver and zinc nanoparticles. The interaction between the chemical moieties present in DGL—SNPs and DGL—ZNPs formulated were studied, which revealed the presence of two main vibrations (i.e. stretching and bending) in the wavelength range of 4000 – 500 cm^{-1} as shown in Figure 4 and Table 1.

For DGL—SNPs (Figure 4a and Table 1), the peak positions at 3215.398 cm^{-1} represents the N—H functional group while the peak around 3365.97 cm^{-1} corresponds to the O–H groups of tannins, flavonoids, phenolic compounds, glucose and –NH stretching of proteins (Elemike *et al.,* 2017). Bands presenting at the 2850—3000 cm^{-1} region indicates the C—H stretching of alkanes, while the peak around 1625 cm^{-1} is due to the enolic β-diketones or —C=O stretch of carboxylic acids cm^{-1} (Elemike *et al.,* 2017). The assignment of peaks is similar to other literature reports (Tripathy et *al.,* 2010; Verma and Mehata, 2016). The appearance of these peaks suggests the presence of phytochemicals such as flavonoids, alkaloids, phenolics, organic acids of the *Dialium guineense* leaf extract in the DGL—SNPs, which are responsible for stabilizing as well as the capping effects on the nanoparticles. The biomolecules may have interacted with the Ag ions through their oxygen donor atoms and are adsorbed on the surface of the metal ions which is manifested by a decrease in the peak intensities of bands observed in the DGL—SNPs (Elemike *et al.,* 2017).

Similar peaks were observed for DGL—ZNPs (Figure 4b and Table 1), the band around 1625 cm^{-1} are assigned to the enolic β-diketones or —C=O stretch of carboxylic acids cm^{-1} of the IR spectrum (Elemike *et al.,* 2017). A strong peak inentsity corresponding to the C—H stretch of alkanes was also observed. The

peak positions at 3273.6 cm^{-1} represents the N—H functional group while that at 3047.8 cm^{-1} is assigned to the C=C functional group of unsaturated alkenes. the peak around 3364.567 cm^{-1} corresponds to the O–H groups of tannins, flavonoids, phenolic compounds which show characteristics peak position at 3350 cm^{-1} . The listed observations of bands gave the confirmation of proteins and amino acids in the capping agents of the Zinc oxide nanoparticle (DGL—ZNPs). Thus, the proteins around the $Zn(NO3)_2$ act as reducing, capping

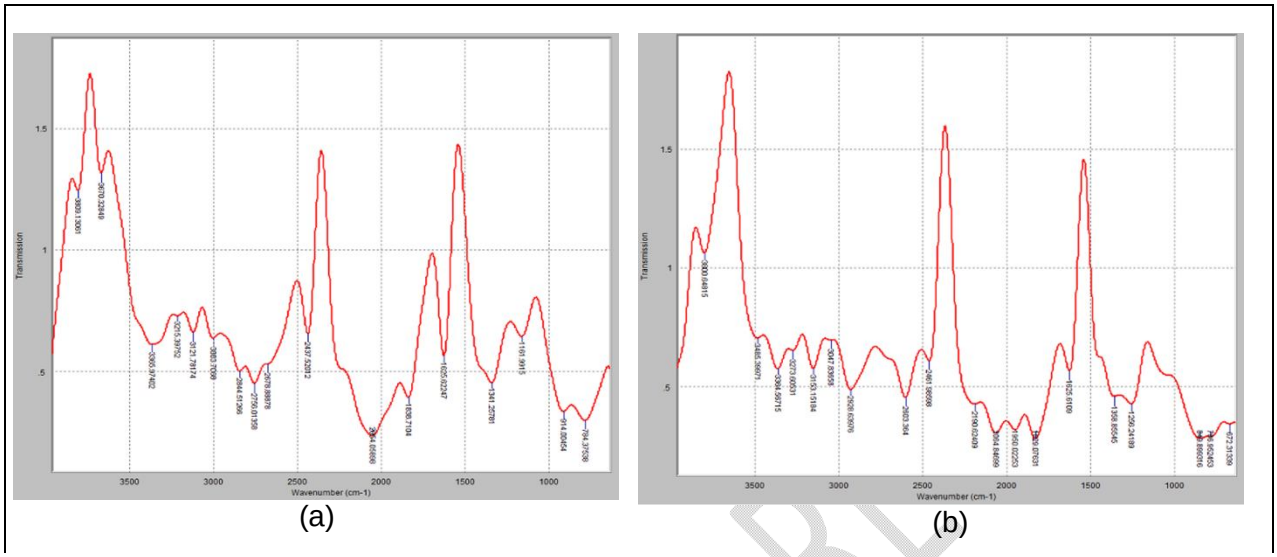

(a) (b)

and stabilizing agents during the synthesis of the DGL—ZNPs.

Figure 4 FTIR graph of (a) DGL—SNPs and (b) DGL—ZNPs

Table 1: Peak number along with Wave number of FTIR graph of DGL—SNPs and DGL—ZNPs

DGL—SNPs		DGL—ZNPs	
Peak number	**Wavenumber (cm^{-1})**	**Peak number**	**Wavenumber (cm^{-1})**
1	784.3754	**1**	672.3134
2	914.0045	**2**	786.9525
3	1161.992	**3**	849.8993
4	1341.258	**4**	1256.242
5	1625.622	**5**	1358.855
6	1838.71	**6**	1625.611
7	2054.059	**7**	1829.076
8	2437.52	**8**	1950.023
9	2678.889	**9**	2064.847
10	2758.014	**10**	2190.624
11	2844.513	**11**	2461.986
12	3003.707	**12**	2603.364
13	3121.782	**13**	2928.64
14	3215.398	**14**	3047.837
15	3365.974	**15**	3153.152
16	3670.328	**16**	3273.605
17	3809.131	**17**	3364.567
		18	3485.4
		19	3800.648

3.5. ANTIMICROBIAL ASSAY OF DGL—SNPS AND DGL—ZNPS

The formulated test agents, DGL—SNPs and DGL—ZNPs were found to show momentous action against microbial test organisms (Table 2), especially for the *P. mirabilis* organism. Figure 5 and 6 collectively shows the antimicrobial activities of DGL—SNPs and DGL—ZNPs against human pathogens. Growth inhibition profile of DGL—SNPS and DGL—ZNPS on *P. mirabilis* are presented in Figure 5 a. One-way ANOVA of the IC_{50} (the concentration of test agents required to elicit a 50 % inhibitory response in the growth of the test organisms) of DGL—SNPS and DGL—ZNPS was done at $P < 0.05$. Figure 6a shows significant mean difference between DGL—SNPs and DGL—ZNPs; the synthesized silver nanoparticles presented improved outcome to the DGL—ZNPs with a *P* value of 8×10^{-4}. Even though Gugale *et al*. did not do a comparative evaluation of the antimicrobial efficacies of different metal nanoparticles using green synthesis method, they established that enhanced antimicrobial property of silver nanoparticles (Gugale *et al*., 2021)

Table 2. Zone of inhibition (ZI) and Minimum inhibitory concentration (MIC) of DGL—SNPs and DGL—ZNPs

Test organism	Mean of ZI (mm) of test agents								MIC (mg/ml)	
	100 mg/ml		50 mg/ml		25 mg/ml		12.5 mg/ml			
	[a]	[b]	[a]	[b]	[a]	[b]	[a]	[b]	[a]	[b]
Staphylococcus aureus	10	15	0	0	0	0	0	0	20	10
Escherichia coli	15	9	10	0	0	0	0	0	10	5
P. aeruginosa	13	12	9	0	0	0	0	0	10	5
Proteus mirabilis	10	18	8	0	0	0	0	0	5	2.5
Klebsiella sp	12	9	10	0	0	0	0	0	2.5	5
S. pneumoniae	12	12	8	0	0	0	0	0	5	5
Candida albicans	10	12	0	0	0	0	0	0	20	10

[a] Zinc oxide nanoparticle [b] Silver nanoparticle

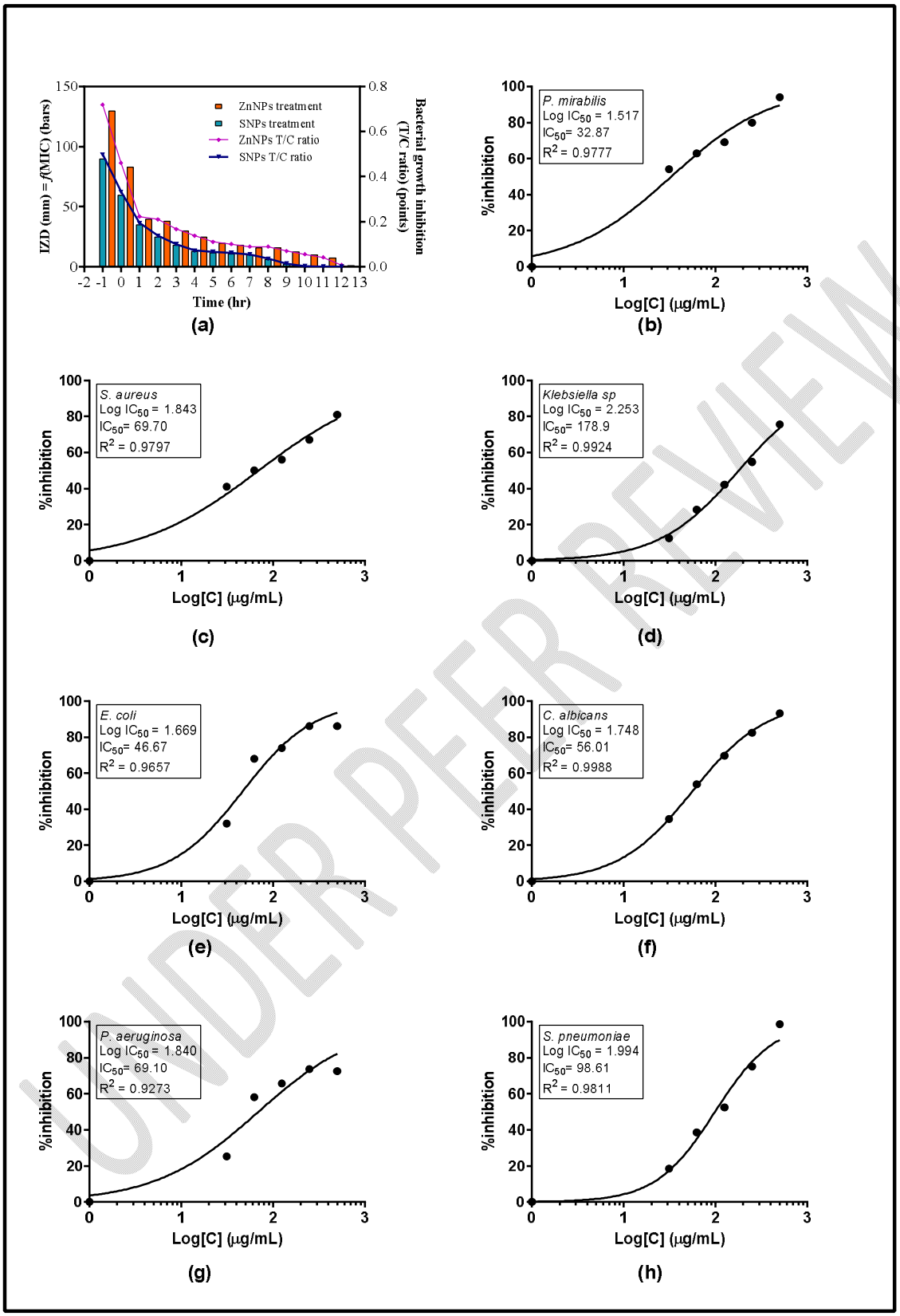

Figure *5.* (a) Growth inhibition profile DGL—SNPs and DGL—ZNPs on *P. mirabilis,* (b—h) IC_{50} of DGL—ZNPs for each of the organism

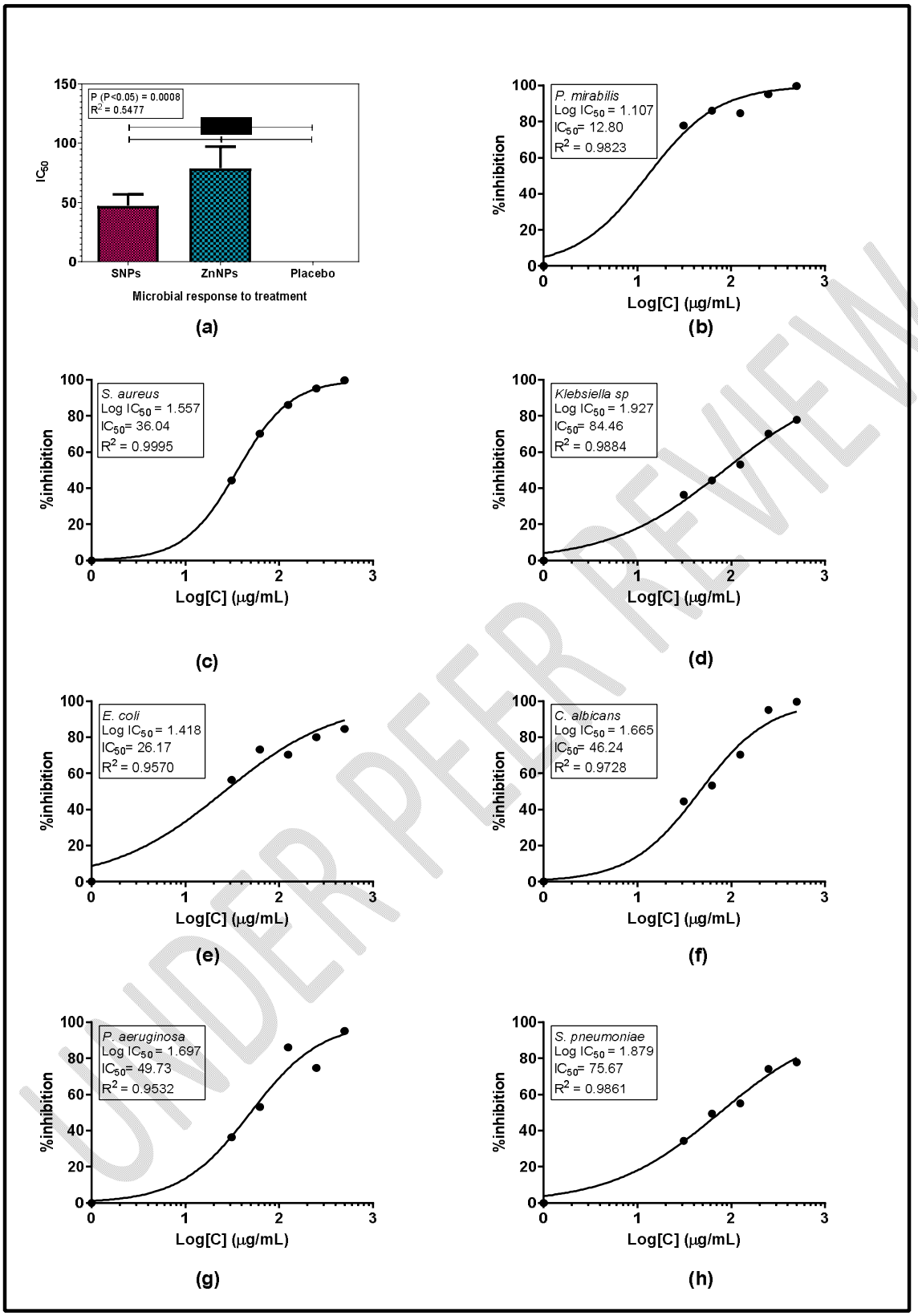

Figure 6 (a) One way ANOVA of the IC_{50} of DGL—SNPs and DGL—ZNPs, (b—h) IC_{50} of DGL—SNPs for each of the organism

4. CONCLUSION

Green synthesis of DGL—SNPs and DGL—ZNPs from the leave extract of *Dialium guineense* plant is the latest alternative to a chemical and physical synthesis sequel to its novel toxicity free, eco-friendly and biocompatibility. This work reported the biogenic synthesis and comparative assessment of the antimicrobial activities of silver nanoparticles and zinc nanoparticles of DGL against human pathogens. The respective reduction of silver and zinc ion to silver and zinc atom was observed by UV visible with SPR peak at about 275 nm and 261 nm. The XRD analysis confirmed the highest peak of DGL—SNPs and DGL—ZNPs crystals correspond to (0 1 3) and (1 2 2) diffraction plane respectively. The SEM confirmed a spherical morphology for DGL—SNPs, and a hexagonal for DGL—ZNPs. The FTIR analysis indicates that the metabolites in DGL are responsible for the bio-reduction in the synthesis of DGL—SNPs and DGL—ZNPs. Thus, the protein in the extract played an important role in the stabilization of the silver and zinc. The silver nanoparticle presented better antimicrobial inhibition in comparison to the synthesized zinc nanoparticles. It is thus a promising antimicrobial agent against human pathogens.

DISCLAIMER (ARTIFICIAL INTELLIGENCE)

Author(s) hereby declare that NO generative AI technologies such as Large Language Models (ChatGPT, COPILOT, etc.) and text-to-image generators have been used during the writing or editing of this manuscript.

REFERENCES

Akpomie KG, Ghosh S, Gryzenhout M, Conradie J (2021). One-pot synthesis of zinc oxide nanoparticles via chemical precipitation for bromophenol blue adsorption and the antifungal activity against filamentous fungi. Scientific reports. Apr 15; 11(1):8305. https://www.nature.com/articles/s41598-021-87819-2

Bankier C, Matharu RK, Cheong YK, Ren GG, Cloutman-Green E and Ciric L (2019). Synergistic Antibacterial Effects of Metallic Nanoparticle Combinations. *Scientific Reports*, **9**:16074. https://doi.org/10.1038/241598-019-52473-2

Crane JK (2020). Metal Nanoparticles in Infection and Immunity. *Immunological investigations*, **49**(7): 794-807. https://doi.org/10.1080/08820139.2020.1776724

Dizaj S M, Lotfipour F, Barzegar-Jalali M, Zarrintan M H and Adibkia K. (2014). Antimicrobial activity of the metals and metal oxide nanoparticles *Mater. Sci. Eng*. *C* **44**: 278–84

Elemike EE, Fayemi OE, Ekennia AC, Onwudiwe DC, and Ebenso EE (2017). Silver Nanoparticles Mediated by *Costus afer* Leaf Extract: Synthesis, Antibacterial, Antioxidant and Electrochemical Properties. *Molecules,* **22**:701

Filho A, Dos Santos S, Dos Santos MS, Backx OAL, Soran BP, Opriş ML, Lung O, Stegarescu, I and Bououdina M (2023). Biosynthesis of Nanoparticles Using Plant Extracts and Essential Oils. *Molecules (Basel, Switzerland)*, *28*(7), 3060. https://doi.org/10.3390/molecules28073060

Gao W, Chen Y, Zhang Y, Zhang Q and Zhang L (2018). Nanoparticle–based local antimicrobial drug delivery. *Adv. Drug Delivery Rev*., **127**, 46–57 https://doi.org/10.1016/j.addr.2017.09.15

Gugale GS, Bhusare BP, Ambawade MS, Kadam NS, and Shinde AB (2021). Biosynthesis of Silver Nanoparticles using various botanicals and evaluation of its antimicrobial property. *Jour Pl Sci Res*., **37**(2):507-15. DOI: https://doi.org/10.46243/jst.2021.v6.i3.pp01-06

iNaturalist (2024). iNaturalist Research-grade Observations. https://doi.org/10.15467/ab3s5x accessed via GBIF.org on 2024-12-05. https://www.gbif.org/occurrence/4522630884

Kalakonda P, Mandal P, Mynepally SL, Bashipangu A, Kethavath A, Khanam SJ, Batchu M, Kalakonda PB, Banne S, Dayanand A, Banavoth M, Kigoji M, Shukla VD, Eluri Y and Bhaskar B (2024). Comparison of Multi-metallic Nanoparticles-Alternative Antibacterial Agent: Understanding the role of their Antibacterial Properties. *Journal of inorganic and Organometallic Polymers ad Materials*, **34:** 2203-2218. https://doi.org?10.1007/s10904-023-02960-x

Karade V C, Patil R B, Parit S B, Kim J H, Chougale A D and Dawkar V V. (2021). Insights into shape-based silver nanoparticles: a weapon to cope with pathogenic attacks ACS Sustain. *Chem. Eng*. **9** (12): 476–507

Khan AU, Malik N, Singh B (2023). Biosynthesis, and characterization of Zinc Oxide nanoparticles (ZnONPs) obtained from the extract of waste strawberry. *J.Umm Al-Qura Univ. Appll. Sci.* **9:**268-275. https://doi.org/10.1007/s43994-023-00038-5

Kim JS, Kuk E, Yu KN, Kim JH, Park SJ, Lee HJ, Kim SH, Park YK, Park YH, Hwang CY. (2007). Antimicrobial effects of silver nanoparticles. *Nanomed. Nanotechnol. Biol. Med*., **3**: 95–101

Ma X, Zhou S, Xu X, and Du Q. (2022). Copper-containing nanoparticles: Mechanism of antimicrobial eefect and application in dentistry0a narrative review. *Frontiers in surgery,* **9**, 905892. https://doi.org/10.3389/fsurg.2022.905892

Marhaba S (2018). Effect of size, shape and environment on the optical response of metallic nanoparticles. *InTech.* DOI: 10.772/intechopen.71574

Mirel S, Pusta A, Moldovan M and Moldovan S (2022). Antimicrobial Meshes for Hernia Repair: current Progress and Perspectives. *Journal of clinical medicine,* **11**(3):883. https://doi.org/10.3390/jcm11030883

Mondal SK, Chakraborty S, Mannab S, and Mandal SM. (2024). Antimicrobial nanoparticles: current landscape and future challenges. RSC Pharm., **1**, 388 DOI: 10.1039/d4pm00032c

Okeniyi JO, John GS, Owoeye TF, Okeniyi ET, Akinlabu DK, Taiwo OS, Awotoye OA, Ige OJ and Obafemi YD (2017). Effects of *Dialium guineense* based zinc nanoparticle material on the inhibition of microbes inducing microbiologically influenced corrosion. In Proceedings of the 3rd Pan American Materials Congress (pp. 21-31). Springer International Publishing. https://link.springer.com/chapter/10.1007/978-3-319-52132-9_3

Pashazadeh-Panahi P and Hasanzadeh M (2020). Digoxin as a glycosylated steroid-like therapeutic drug: Recent advances in the clinical pharmacology and bioassays of pharmaceutical compounds. *Biomedicine & Pharmacotherapy,* **123:** 109813 https://doi.org/10.1016/j.biopha.2020.109813

Punjabi K, Mehta S, Chavan R, Chitalia V, Deogharkar D and Deshpande S (2018) Efficiency of Biosynthesized Silver and Zinc Nanoparticles Against Multi-Drug Resistant Pathogens. *Front. Microbiol.* 9:2207. doi: 10.3389/fmicb.2018.02207

Raja FNS, Worthington T, and Martin RA. (2023).The antimicrobial efficacy of copper, cobalt, zinc and silver nanoparticles: alone and in combination. *Biomed. Mater*. 18 045003 https://doi.org/10.1088/1748-605X/acd03f

Rather GA, Hassan S, Pal S, Khan MH, Rahman HS, and Khan J (2021). Antimicrobial Efficacy of Biogenic Silver and Zinc Nanocrystals/Nanoparticles to Combat the Drug Resistance in Human Pathogens. *Intechopen* DOI: http://dx.doi.org/10.5772/intechopen.99200

Salazar-Aleman DA and Turner RJ (2022). Meal based Antimicrobials: Uses and Challenges. In: Hurst CJ (eds) Microbial Metabolism of Metals and Metalloids. Advances in Environmental Microbiology, vol 10. *Springer, Cham*. https://doi.org/10.1007/978-3-030-97185-5_4

Shaalan, M.I., El-Mahdy, M.M., Theiner. (2017). In vitro assessment of the antimicrobial activity of silver and zinc oxide nanoparticles against fish pathogens. *Acta Vet Scand* **59**, 49 https://doi.org/10.1186/s13028-017-0317-9

Shnawa, B. H., Jalil, P. J., Al-Ezzi, A., Mhamedsharif, R. M., Mohammed, D. A., Biro, D. M., & Ahmed, M. H. (2024). Evaluation of antimicrobial and antioxidant activity of zinc oxide nanoparticles biosynthesized with Ziziphus spina-christi leaf extracts. *Journal of environmental science and health. Part C, Toxicology and carcinogenesis*, *42*(2), 93–108. https://doi.org/10.1080/26896583.2023.2293443

Ventola C L (2015). The antibiotic resistance crisis: part 1: causes and threats *Pharm. Ther*. **40** 277

Vincent M, Hartemann P and Engels-Deutsch M (2016). Antimicrobial applications of copper. *International journal of Hygiene and Environmental Health*, **219** (7):585-591. https://doi.org/10.1016/j.ijeh.2016.06.003

Yilmaz, Dilek Koca, Fatih Ertas, Nurhan (2019). Comparison of antimicrobial activity of bio-synthesized silver and zinc oxide nanoparticles using *Lavandula stoechas* leaf extract. *Research journal of biotechnology*, **14**

Yoo A, Lin M, Mustapha, A. (2021) Zinc Oxide and Silver Nanoparticle Effects on Intestinal Bacteria. *Materials*, **14**, 2489. https://doi.org/10.3390/ma14102489

Zou J, Fan c, and Liu X (2020). Effect of Molecular Cross-sectional Areas of Adsorbed Nitrogen on the Brunauer-Emmett-Teller Analysis for Carbon—based Slit Pores. *Langmuir,* **36**(48): 14656-14665. https://doi.org/10.1021/acs.langmuir.0c02514